SAND83-1150 Distribution
Unlimited Release UC-94e
Printed September 1983

A USER'S MANUAL FOR THE SALT SOLUTION MINING CODE, SANSMIC

Anthony J. Russo
Fluid Mechanics and Heat Transfer Division 1512
Sandia National Laboratories
Albuquerque, New Mexico 87185

ABSTRACT

SANSMIC is a computer code used to predict the development of axisymmetric caverns which are solution mined in salt formations. It was written to aid in the design and operation of Strategic Petroleum Reserve oil storage caverns. For a prescribed leaching schedule, the code calculates volume and shape changes, including the case of leaching during oil injection (leach-fill) and withdrawal by fresh water displacement. This manual contains a brief description of the models used in SANSMIC, some comparisons with field data, and detailed instructions for the use of the code as it is currently configured to run on the Sandia CRAY, VAX 11/780, and Cyber 76 computing systems.

CONTENTS

LIST OF FIGURES

INTRODUCTION

The United States Strategic Petroleum Reserve (SPR) consists of an underground oil storage system which uses caverns leached in salt domes near the Gulf of Mexico and a former salt mine on Weeks Island, Louisiana. Some of the cavern space, formed during commercial brining operations, was available for storage shortly after the program began; however, since this space was less than 250 million barrels, and storage of up to 1 billion barrels is being considered, the Department of Energy (DOE) has undertaken an extensive solution mining program.

The new leached caverns will each hold 10 million barrels of oil. They are approximately 2000 feet tall with the cavern roofs set several thousand feet below the surface. The caverns are designed to accommodate five withdrawal cycles of oil with the oil being displaced by fresh water. Therefore, initially, the bottom diameter (160 feet) is made smaller than the top diameter (240 feet) so that the shape will not deviate significantly from cylindrical during the cavern lifetime.

Because there was urgency to fill the reserve as rapidly as possible, considerable attention was given to devising a leaching scheme which would yield not only the desired size and shape of cavern but would do it in the shortest practical time. At one time this appeared to be accomplished best by using a leach-fill strategy in which the cavern would be simultaneously filled with oil as the leaching proceeded. To start the cavern, several wells could be drilled and simultaneously leached until the cavities coalesced to form a sump.

The need to model the solution mining process in order to plan and develop these new caverns was obvious. However, because no project of this magnitude had ever been attempted before, confidence in existing models had to be tempered. One of the tools which had been successfully used to develop smaller caverns was the SMRI code SALT77 described in Reference 1. This code proved very useful for planning some portions of the leaching program and developing early leaching schedules. The need to handle moving blanket problems (necessary in leach-fill and oil withdrawal analyses), which SALT77 was not structured to do, and to perform a very large number of calculations

efficiently, led to the development of a new code, SANSMIC, which utilizes the same dissolution model as SALT77, but which includes new diffusion, plume, and insolubles models and uses an implicit numerical formulation. This report describes the models used in SANSMIC, some examples of its application to the SPR program, and instructions on the use of the code.

SANSMIC users are CAUTIONED that the models employed in this code are steady-state or quasi-steady models and that the code has only been verified with experimental data from SPR caverns which have large length-to-diameter ratios. These caverns were leached with flow rates in the 10^5 barrel per day range. Operation in a different flow rate or geometry range may not give similar accuracy. In particular, laboratory and field experience indicates that water injected in short bursts, after which the enclosure is allowed to stabilize, rises to the top of the enclosure with little mixing and tends to etch out a narrow disk just below the blanket or pad. SANSMIC will not model this behavior properly.

THEORY

Basic Equations.

The details of the theory used in developing the computer code **SANSMIC** are contained in Reference **2,** however, for the reader's convenience a brief description of the basic equations and models used will be included here.

When a vertical salt surface is exposed to unsaturated brine, a negatively buoyant dissolution boundary layer is formed next to the surface. Figure 1 shows the geometry and flow regions in a cavern. Application of a momentum integral analysis to this boundary layer and a series of verification experiments by Durie and **Jessen**[3,4] showed that when the peak fall velocity of this boundary layer was large compared to the edge or bulk velocity of the brine, the dissolution rate at a given temperature varied only with the bulk concentration of the brine and the distance along the boundary layer. Their experiments also showed that the transition to turbulence occurred in very small length scales (typically millimeters). By analogy with turbulent heat transfer by natural convection on a long vertical surface, the distance dependence of the dissolution rate could be **neglected**[5]. The salient results of this dissolution analysis are summarized in Reference 1.

The recession rate of a large vertical wall of salt dissolving under the influence of natural convection can be correlated as a function of only the bulk fluid specific gravity, C, at temperatures near **75°F.**

$$\frac{dr}{at}\ (\text{ft/hr}) = 45.654996\ C^4 - 232.29310\ C^3 + 469.52470\ C^2 - 470.37554\ C + 232.73686 - 45.203241\ /C \qquad (1)$$

The recession rate varies with wall angle, θ, measured from the vertical so that θ = **90°** is an upward facing surface and θ = **-90°** is a downward facing surface, according to:

$$\left.\frac{ar}{at}\right|_{\theta \geq 0} = \left.\frac{dr}{at}\right|_{\theta=0} \left[\cos\left(\frac{\theta}{3}\right)\right]^{1/2}$$

$$\left.\frac{ar}{dt}\right|_{\theta<0} = \left.\frac{dr}{at}\right|_{\theta=0} \left\{1 + 0.22\left[1 - \sqrt{\frac{\theta + 45°}{45°}}\right] - \frac{45°}{45°}\right\} \qquad (2)$$

To use these recession rate correlations to calculate cavern formation shapes, the specific gravity of the brine as a function of height must be determined.

If it is assumed that, except for the buoyant plume region above the fresh water injection point and the salt surface boundary layer, the radial concentration gradient is negligible, the theory of stratified enclosures can be used to find C.

Rahm and Walin[6,7,8] have developed an approximate theory for treating combined natural and forced convection in stably stratified enclosures where the natural convection is induced by wall sources weak enough so that the thermal or concentration boundary layer variations are smaller than the total variation due to stratification. The result of this analysis is that the variation of specific gravity with height in the bulk of the fluid is given by Equation (3) for axisymmetric caverns.

$$\frac{\partial C}{\partial t} + \left(\frac{M_o}{A} - \frac{2D}{r}\frac{dr}{dz}\right)\frac{\partial C}{\partial z} + \frac{2DS_d\,(C - \hat{C})}{r\cos\theta} = D\,\frac{\partial^2 C}{\partial z^2} \qquad (3)$$

where M_o is the total externally induced volume flow rate

A is the cavern cross sectional area

D is the diffusion coefficient of salt in water

r is the cavern radius

z is the vertical distance from the cavern bottom.

S_d is a source coefficient defining the wall boundary condition by $\left.\frac{\partial C}{\partial \xi}\right|_{\xi=0} = S_d\,(C - \hat{C})$

$\hat{C}$ is the specific gravity of the fluid at the wall ($\xi = 0$). Taken to be the saturation value of 1.202.

t is time

and θ is the wall angle with respect to vertical.

Equation (3) is a mass conservation equation which balances the rate of salinity increase (first term) with the sum of the net convective flux (second term), the rate of salt dissolution at the walls (third term) and the diffusive flux (last term).

Equation (3) holds outside the plume region above and below the stagnation level (the level at which the buoyant plume grows large enough to interact with the walls, see Fig. 1). At the stagnation level the value of specific gravity is used as a boundary condition for the solution of Equation (3) along with a zero derivative condition at the upper boundary and a saturation condition at the lower boundary. The stagnation level specific gravity is determined by a mass balance between the injected fluid, and dissolved and diffused salt in a control volume. For either reverse leaching (injection point above the production point) or direct leaching (injection point below the production point) the control volume is the region between the injection and stagnation levels. The stagnation level is estimated from a simple unconstrained buoyant plume model.

Plume Model.

Since the mixing within the plume is usually rapid, an analysis of plume dynamics based on the assumption of a uniform specific gravity and velocity within the plume (top-hat model) is appropriate. Morton[9] presents the results of such an analysis as a set of equations which describe the dynamics of an unconstrained steady plume.

$$\frac{d\,(b^2\,u)}{dz} = 2\alpha b u$$

$$\frac{d\,(b^2\,u^2)}{dz} = 2\,b^2 g\,(C_o - C) \qquad (4)$$

$$\frac{d\,(b^2\,ug\,(C_o - C))}{dz} = 2\,b^2\,ug\,\frac{d\,C_o}{dz}$$

where b is the effective plume radius
C and C_o are fluid specific gravities in and out of the plume
u is the plume velocity in the vertical (z) direction
g is the acceleration of gravity
and a is an entrainment coefficient.

When the plume is rising through a stably stratified fluid ($\partial C_o/\partial z < 0$) it will rise to a certain level and stop, and its radius will grow indefinitely. This level is denoted by the plume stagnation level in Figure 1. If the plume is rising in an unstably stratified fluid, it will continue to rise and grow until it interacts with the cavern walls which then constrain the plume and change its rise rate. The level at which this interaction occurs (the level at which the plume radius equals 0.7 of the cavern radius) will also be denoted as the plume stagnation level, because in either case the entire plume flow is deposited in the fluid cell containing this level.

Diffusion Model.

The diffusion coefficient, D, which appears in Equation (3) is a strong function of whether the brine is stably or unstably stratified. For stable concentration gradients, D is just the molecular diffusion coefficient, D_{mol}, which is very small (1.4×10^{-5} cm^2/sec). However, when the concentration gradient is positive (unstable case), a much larger eddy diffusion coefficient, D_e, must be used. An instability analysis given in Reference 2 indicates that an appropriate mixing length, ℓ, to use in calculating D_e when wall effects are ignored is

$$\ell = \left(\frac{6\pi}{\alpha}\right)^{3/4} \left(\frac{2\nu^2 C}{\frac{dC}{dz} g}\right)^{1/4} \qquad (5)$$

where α is the entrainment coefficient

ν is the local kinematic viscosity of the brine

and g is the gravitational acceleration.

If it is assumed that the eddy diffusion coefficient is proportional to the product of velocity and mixing length, and the mixing length is taken as the minimum of cavern radius r and ℓ (as given in (5))

$$D_e = D_o \, (dC/dz)^{1/2} \, \text{Min} \, (r^2, \ell^2) \qquad (6)$$

Equation (6) is the final form of the eddy diffusion coefficient to be used in Equation (3) where $D = D_{mol} + D_e$. The value of D_o used was 31.7 $ft^{1/2}/sec$ taken from the data of Reference 10, and the value of α in Equation (5) which best fit a limited amount of data taken from Bryan Mound well 104 was 0.064. This value of α is not far from other experimentally determined values for buoyant plumes which are typically about 0.08.[9]

Insolubles Model.

Part of the input data required to run SANSMIC is the specification of the volume percent of insolubles in the salt formation. A sample of salt from the dome at Bryan Mound, Texas, was analyzed to determine the insoluble particulate size distribution. Most of the insolubles were anhydrite particles between 20 and 400 micrometers average diameter, with a peak at 250 micrometers. Assuming Stokes drag on spherical particles, the settling velocity for each particle size over the range 0 to 400 micrometers was calculated and the integrated fraction that would fall out in an upward velocity field was calculated as a function of fluid velocity. A curve fit to these results, Equation (7), is included in the code to establish the fraction of insolubles that fill the cavern sump or are discharged.

$$f = 0.5/(1 + 0.00231\ v) + 0.5\ e^{-0.002v} \qquad (7)$$

where f is the total fall fraction

and v is the upward fluid velocity (ft/hr).

The code keeps account of the insolubles that fall and raises the sump floor accordingly as well as increasing the wall recession rate in proportion to the insolubles freed at each level.

Numerical Method.

The cavern space to be solution mined is divided into N equal Sized vertical increments with a mesh point located at each of the N + 1 boundary planes. All values within an increment are assumed to be represented by the value at its lower boundary. The initial radius and concentration for each increment, the oil-brine interface level, injection and production levels, and the injection flow rate are defined for each case.

At every third time step the Equations (4) are solved, using the Sandia system library integration routine ODE, for the plume concentration, flow rate, and stagnation level. At each time step the concentration in the mesh increment containing the stagnation level is updated by a mass balance between the injected fluid, the remaining brine in the increment volume, and the salt which diffused and dissolved during one time step. This concentration serves as one of the boundary values for the solution of Equation (3) above and below the stagnation level.

All the terms except the convective one in Equation (3) are implicitly center differenced in conservation form. Upwind differencing is used on the convective term. The difference equations are solved with a tridiagonal algorithm. The diffusion coefficient is a function of specific gravity gradient and is calculated by

$$D = D_{mol} + D_o \left(\frac{dC}{dz}\right)_+^{1/2} \text{Min}\,(r^2, \ell^2) \qquad (8)$$

where D_{mol} is the molecular diffusion coefficient, $(dC/dz)_+$ is the specific gravity gradient when positive, and is zero when the specific gravity gradient is negative. The coefficient D_o is an empirically determined eddy diffusion parameter, and the mixing length ℓ is determined from Equation (5) with $a = 0.064$.

After the solution of Equation (3), the new concentrations are used to calculate the wall recession rate from Equations (1) and (2). The cavern radii are updated and the coefficients of Equation (3) reevaluated in preparation for the next time step.

Since the plume Equations (4) and the concentration Equation (3) are tightly coupled and solved sequentially, some numerical oscillation or bouncing of the plume stagnation level can occur. In order to stabilize the plume and limit the errors due to this oscillation, the stagnation level has been restricted to lie within two mesh intervals below the level previously calculated (it can fall by only two spaces at a time). Since the time required for the plume to find a stable level is small compared to the leaching time, this approximation should introduce little error.

The solution to any differential equation is determined by its boundary conditions. The boundary condition at the stagnation level is computed at each time step from the values at the previous time step and errors tend to accumulate. The cavern volume and shape are very sensitive to the boundary values used, so it is important to limit the errors on these values. This is accomplished by performing a global mass balance at each time step and computing a correction factor for the concentrations and boundary conditions to be used in the next time step. This forces the mass concentration in the time integration to follow a self-consistent and self-correcting path.

The total mass of brine in the cavern, UT, is computed by the time integral

$$M_T = m_{co} + \int_0^T \left(\sum_1^N \frac{VSR}{\Delta t} C_{salt} + Q_i C_i - (Q_o + Q_{fill}) C_p \right) dt \quad (9)$$

where Q_o is the outlet volume flow rate for no oil flow

Q_{fill} is the oil volume flow rate

C_p is the brine S.G. at the production level

T is the time period

VSR is the volume of salt removed from the increment Az in the time increment At

m_{co} is the initial mass of brine in the cavern

and N is the number of mesh intervals used.

The total mass of brine in the cavern, M_c, can also be computed by

$$M_c = \sum_{I=1}^{N} \pi r^2(I) \, \Delta z \, C(I) \quad (10)$$

and the correction factor for the stagnation level boundary condition is then found by

$$\text{Corr. Fac} = \frac{M_T}{M_c} \quad (11)$$

This factor is always close to 1 and is printed out with each result. A value of 1 for the correction factor only means, of course, that the calculation is self-consistent, and not that it is modeling any physical situation correctly.

Dissolution Rate Correction.

When the previously described models and numerical method are compared to field data, it is found that for cases in which reverse leaching is employed, with the injection point well below the protective roof oil blanket, the dissolution rate is larger than predicted by Equation (1). It is believed that this occurs because, as is noted at the beginning of the Theory section, the dissolution correlations are only valid when the bulk fluid flow velocities are much less than the peak boundary layer velocity. For the case described above, the plume rising near the center of the cavern and the return flow along the periphery generate a toroidal vortex, the velocity of which may be much greater than that calculated for plain plug flow.

An accurate model of the vortical velocity field, which is a function of raw water injection rate, pipe string settings and cavern geometry, has not yet been included in the code. Instead a model based on heuristic arguments and some empirical fits has been used to calculate a dissolution rate correction term, E_{diss}. For the region between the injection height, Zi, and the oil blanket height, Zb,

$$E_{diss} = 0.0067\ \mathrm{MIN}(L\Delta z/200, 2, R/25)\ Qi\ [(1-L_r)L_r]^{0.25}$$

and below Zi

$$E_{diss} = E_{diss}\Big|_{Zi}\ e^{-2.5\ L_r}$$

where $L_r = L_v/L$

$L = (Zb-Zi)1.15/\Delta z$

$L_v = L-(Z-Zi)/Az$

AZ = length of a vertical mesh increment

and R = cavern radius at the injection level

RESULTS

Comparison with SALT77.

The SMRI code (SALT77) has been verifed for the cases of bottom injection and brine removal at the top (direct leaching) and top injection and bottom brine removal (reverse leaching)'. Since a degree of confidence has been established for the SMRI code for the simple direct and reverse leaching cases, the first comparison to be made will be for leaching through a 0.625 foot radius borehole in the direct mode for 40 days at a flow rate of 10603.5 ft^3/hour (1322 gallons/minute) of water with a specific gravity of 1.0108, and then in the reverse mode at the same flow rate for 100 days. Figure 2 shows a comparison of the cavern shapes calculated with the SMRI code and the new code. The cavern shapes are almost identical differing only near the injection region by about 10%. The overall cavern volumes differed by 5.5% at the end of the mining process. The produced brine saturation percent differed by less than 0.3%.

Bryan Mound Cavern 106.

Data are available from the direct leaching of Bryan Mound Cavern 106. Two wells, A and B, were simultaneously leached for one day at a flow rate of 1507 ft^3/hr, then for 84 days at an average flow rate of 6596 ft^3/hr. The injection water was assumed to have a specific gravity of 1.0108. A 7-inch injection tubing was set at a depth of 4450 feet and a 10.75 inch production casing was set at a depth of 2280 feet. The initial borehole size was taken to be 15 inches in diameter. In actuality, the two wells would eventually coalesce with each other and with a third well started later, thereby forming Cavern 106. All simulations and data discussed here are for the period when each well formed a separate cavity. This case was simulated with both the SMRI code and the new code neglecting insolubles. The results are shown in Figure 3 along with sonar caliper data taken by the Dowel1 Corporation between July 2 and July 6, 1980. The radii data plotted in Figure 3 are effective radii, which, if the cavern cross section were circular give the same area as that measured (the same as the RMS radius). The calculated curves practically fall on each other, differing by 2% or less over the whole depth but both underestimate the measured volume by

about 20%. This discrepancy could be caused by a number of factors. First, the accuracy of the flow measurements is not known. Error estimates of 20% have been made for some measurements. The assumed temperature for all calculations was 75°F but the exit temperature of the brine was as high as 98°F during some of the leaching. The insolubles content was neglected (about 7%). The calculations assume an axisymmetric geometry but the actual cross sections were not circular. This fact can be significant because the larger surface to volume ratios would cause more salt to dissolve than was estimated. The sonar data were taken in eight directions (5% accuracy is typical for radius sonar data), and if the average value of the radii are taken rather than the RMS value, the results are quite different--indicating a large deviation from circularity. Figure 4 shows the average radius data plotted with the calculated values. This plot indicates a better fit and the calculations even seem to overestimate the cavern size slightly. The asymmetries in the dissolution of the cavern can be caused by the presence of highly soluble sylvite deposits, uneven distribution of anhydrite or other insolubles, or uneven convective mixing of the injected water, none of which can be accounted for in an axisymmetric calculation. Considering all the assumptions that were made, the calculated results seem as good as can be expected.

Comparison with Field Data.

Data from two caverns at West Hackberry, LA, which were leached in the direct mode are shown in Figures 5 and 6. Figure 5 shows calculated and measured cavern effective radii after 147 days of leaching with the injection level at a depth of 5000 feet. The calculated and measured volume agree to within 3%, but the calculated radii near the bottom are larger than the sonar measurements by up to 16% near the bottom of the cavern. The average measured flow rate of 123,880 barrels/day* is probably fairly accurate since the volumes agree so well. Since the injection point was, at the end of the flow, buried several hundred feet below the insolubles level, there was a large quantity entrained insolubles suspended in the lower cavern region, which may have reduced the dissolution rate in that region. If that is not the cause of this discrepancy, modifications to the plume mixing and dissolution models should be considered.

*1 barrel = 5.61458 ft^3

Figure 6 shows a similar comparison for cavern WH104 after 156 days of leaching with an average measured flow rate of 138,404 barrels/day. The calculated volume is 12% greater than the measured volume which indicates that the flow measurements are probably high. The same pattern of overpredicting the cavern radii at the lower end, in this case by 20%, is apparent in Figure 6. For smaller diameter caverns, where the depth of insolubles is not so large, this overprediction has not been observed.

After the sump chimney phase of cavern development is finished, the injection level is usually raised to several hundred feet below the cavern roof and the first phase of reverse leaching is begun. Figure 7 shows a comparison of calculated and measured cavern shape for cavern WH101 at the end of this phase (189 days). The calculated and measured volumes are within 2% of each other, but the maximum radii differ by 15%. The calculation near the top of the cavern is strongly influenced by the dissolution rate correction model described in the theory section, and since this is a rough approximation, such deviations can be expected.

Figure 8 shows the same kind of comparison for cavern WH104. In this case, the volumes differ by 4% and the calculated maximum radius is almost exact, however, near the neck of the upper bulb, the calculated radii are up to 25% too large. The injection level was set 200 feet below the oil blanket level in this case.

The injection level for the corresponding stage in Bryan Mound Cavern 106 was set 630 feet below the oil blanket and the comparison between measured and calculated cavern shape is shown in Figure 9. The total measured cavern volume is only 1% less than the calculated value. Near the bottom of the upper bulb, the radii differ by about 20% for the same reasons mentioned previously. In addition to errors in the dissolution rate model, it should be remembered that the cavern radii shown are effective values, and that in some cases, including BM106, the actual cross section deviates markedly from circularity so that the axisymmetric approximation is poor. The difficulty of accurately predicting cavern shape when there is marked deviation from axial symmetry is shown again in Figure 10. Bryan Mound cavern 104 was leached by coalescing three separate wells at the bottom and then leaching from the top down in one well to further enlarge the cavern. SANSMIC, being an axisymmetric code, had to utilize effective radii obtained from composite cavern

volume data which change the physics assumed in the heuristic dissolution model near the top of the cavern. Despite this, the total volume calculated is within 1%. The calculated depth of the upper bulb is about 25% too small however. Unfortunately, there does not appear to be any simple generalization about how the calculations will deviate from the measured radii. Bryan Mound cavern 105 was also coalesced from three wells and the shape comparison is shown in Figure 11. Here the bulb depth is correct but the calculated peak radius is too small. In this case, however, the calculated volume is also 10% too small which indicates that the flow rate data is too low (volume data should be in better agreement). If the flow rate data is adjusted to bring the calculated volume up to the measured value, the shape comparison shown in Figure 12 is quite good.

An example of the use of the code to predict cavern growth during oil withdrawal is shown in Figure 13. 'West Hackberry Cavern 11 is one of the SPR phase one caverns (a cavern produced during commercial brining) which has been filled with oil. The predicted change in cavern shape and volume as the oil is withdrawn by displacement with fresh water and refilled for 5 complete cycles is indicated in this figure. The lower portion of the cavern, which is exposed for the longest time since the oil blanket rises during withdrawal, enlarges at the fastest rate. This type of withdrawal prediction has been made for each cavern to investigate the possibility of cavern coalescence and to evaluate dome subsidence.

CODE USE

Input Variables Description.

The input data for a complete cavern formation or oil transfer process generally consists of one or more data sets in sequence. Each set is made up of several records which describe geometry or flow parameters which remain constant or vary in a specified way for a fixed amount of time. Each data set corresponds to a specific leaching stage (for example, sump, first reverse, etc.). The first data set contains initial geometry and site parameters which are only read once and need not be repeated. Subsequent data sets consist of only four card images.

The first data record contains up to 60 characters of identification, ending with a "$".

The second data record contains values for the nine integer variables NDIV, IDR, IPRNT, IREPT, IRST, IWAIT, NCO, IDATA, and IVOL.

NDIV The cavern is divided vertically into NDIV computational zones. There are NDIV+1 mesh points associated with these zones. The first mesh point value corresponds to the value at the bottom of the first computational zone which is at the bottom of the cavern.

IDR An option selection index which lets the user choose between:

0 = Ordinary leaching (direct or reverse)

1 = Oil withdrawal mode

2 = Simultaneous leaching and oil filling.

IPRNT Every IPRINT time steps (of duration DT hours) a listing of cavern status will be printed out. Regardless of IPRINT, the cavern status listing is printed at the start and end of each stage (a stage is a data set).

IREPT Any change in variables during cavern development requires a new data set. IREPT=1 tells the code that these new data are a continuation of the same cavern; IREPT=0 for the first data set.

IRST At the end of each run, current cavern data are stored on TAPE 3. To restart a computation with the previous stored data set IRST=1; otherwise, IRST=0.

IWAIT There are IWAIT hours of workovers (zero flow rate) scheduled at the end of this stage.

NCO For cases in which identical leaching operations are simultaneously employed in 2 or 3 wells until they coalesce, SANSMIC calculates the development of a single well until some point in the process where at least some portion of the wells have coalesced. In the next stage data set new effective radii are calculated for a single cavern having the same volume as the previous NCO wells. When NCO is greater than or equal to 2, the variable SEP which is the separation of the well centers must also be provided.

IDATA Since sonar data for a cavern are often in the form of cumulative volume versus depth tables, it is convenient to have the option of reading these in directly and having the computer perform the task of converting them to effective radii and interpolating them onto a vertical mesh. Setting **IDATA** = 1 permits this. If the radii are to be read in directly **IDATA** = 0.

IVOL When IVOL kilo barrels of total volume are leached, the leaching will end for the current stage. This permits stage volume instead of time to be the controlling parameter when the time is set to a value larger than that required to leach IVOL kilo barrels. If IVOL is 0, it is ignored.

The above variables are read with a (915) format.

The next record contains 16 floating point variables which describe the stage parameters. All heights are in feet and are measured from the original cavern bottom (the bottom of the borehole). All flow rates are in barrels per day. All times are in hours. The read format is (8E10.2).

ZMAX The total expected height of the cavern. **ZMAX** will be divided into NDIV regions.

ZI The height of the injection string bottom.

ZP The height of the brine production string bottom.

ZB The height of the oil blanket. If not known for a repeat stage enter 0.0.

QI The raw water injection rate.

RPI The inside radius of the inner tubing (inches).

RPO The outside radius of the inner tubing (inches).

RCASI The inside radius of the casing (inches).

RCASO The outside radius of the casing (inches).

SGI The specific gravity of the injected raw water.

SGCF The average specific gravity of the cavern brine (ignored if **IREPT=1).**

DT Computational time increment. Printouts occur every **IPRNTxDT** hours.

TEND The end time for the stage.

QFIL The oil injection rate (set to zero for ordinary leach).

TDLAY During an oil withdrawal, the oil may stick to the cavern walls as it is displaced by water. The time that this retards dissolution is TDLAY. Presently indications are that this should be set to 0.

SEP For the case when **NCO** wells are to be coalesced, SEP is the separation (feet) between the well centers. When **NCO** is less than 2, SEP is ignored.

Following the first four card image data set (when **IREPT=0)** geometrical data must be supplied. The initial cavern radius at **NDIV+l** mash points must be read in or if **IDATA** has been set to 1, then depth and cumulative (from the cavern roof) volume **(bbls)** must be read in from the bottom up.

For IDATA=O:

NDIV+l radius values are read into the array RC with an **8El0.2** format.

For **IDATA=l:**

The number of depth, volume data pairs is read into NDATA with an 15 format (1 card image). NDATA values of the depth are read into the variable array DEPTH with an **8El0.l** format. NDATA values of the cumulative volume (starting with the largest) are read into the variable array YYY with an **8El0.l** format.

The final record of the first data set (for any value of **IDATA)** consists of four variables: ZDIS, ZFIN, REFDEP and DEPTH which are read in a **4El0.2** format.

ZDIS The average salt dissolution factor (ratio of actual vertical Wall dissolution rate to the model value). Unless special salt characteristics are known, this value should be set to 1.

ZFIN is the average volume ratio of insolubles to salt.

REFDEP is a reference depth at which the plot abscissa begins (on code versions in which the plot routines **are** operative).

DEPTH is the depth of the cavern bottom.

After the first data set has been read in, subsequent four card image sets with **IREPT** set to 1 can be used to continue the cavern development or withdrawal process.

In oil withdrawal mode (IDR=1), the production string level ZP may be set to the blanket level ZB and the time may be set to a large value. The withdrawal stage will end when the oil blanket rises to the cavern roof.

An example of an input data set is shown in Figure 14.

Output Listings.

The code will print out the input data for each stage with an 15 format for the option card image and a 8F10.3 format for the other variables.

At each print interval determined by NPRNT and the time step DP, the following information is printed out:

The time into a particular stage. This quantity is labeled TIME.

The time step DT.

The START TIME of the stage (the start time plus the time is the actual time from the start of the computation).

Six columns of numbers which represent the variation with height up the cavern of effective cavern radius, brine specific gravity, wall angle, flow rate, and cumulative cavern volume from the top down (barrels). The flow rate, which is only listed between the stagnation and brine production levels, is positive in the upward direction and is in barrels per day.

At the bottom of the column listing these additional quantities are printed out.

TOTAL VOLUME	is the total free volume (that which contains a fluid) of the cavern.
BRINE OUT	is the flow rate of brine out of the cavern; it is a few percent less than the injection rate because of the difference between the volume creation rate and the brine expansion rate. PERCENT SATURATION is the product of two factors: the ratio of the dissolved salt weight fraction to the saturation weight fraction, and the ratio of the brine specific gravity to the saturation specific gravity.
VOLUME OF INSOLDBLES	is the volume of insolubles (BBLS) that have fallen into the sump.

VINS VENTED — is an estimate of the height of the fallen insolubles layer above the original cavern (borehole) bottom.

VOL OF INS VENTED — is an estimate of the volume (BBLS) of insolubles vented based on fixed size distribution model.

BLANKET LEVEL — is the height of the oil blanket above the original cavern bottom.

BRINE VOLUME — is the volume of the cavern occupied by brine. (TOTAL VOLUME-BRINE VOLUME is the volume of oil in the cavern.)

CFAC — is a correction factor on the specific gravity boundary conditions which insures a self consistent calculation. It should remain near a value of 1.0. If it does not, the calculation is not reliable.

In addition to the printed output, a separate output file is written onto logical unit 3 (or TAPE 3). This file is written in binary and contains the information needed to continue the run into the next stage or to restart and continue the calculation at a later time.

The present version of the code contains plot calls which utilize the DISSPLA routines rented from Integrated Software Systems Corporation. These calls have been inactivated by conversion to comment statements in versions of the code which do not operate on systems where these plots packages are available.

An example of the printed output for a single time, corresponding to the input of Figure 14, is shown in Figure 15.

CONCLUSIONS

The solution mining code SANSMIC has been developed for calculating the formation of storage caverns in salt. It is applicable to axisymmetric caverns having a single injection and production level. The code uses a vertically stratified mass balance model to calculate the bulk brine salinity which is coupled with an unconfined plume model and an empirical dissolution model to determine the wall recession rate. SANSMIC has options for leaching with or without motion of the oil blanket so that leach-fill or oil withdrawal operations can be simulated. The raw water injection options include direct, reverse and zero flow conditions. If knowledge of the local insolubles content or relative salt dissolution rate is available, it can be incorporated into the calculations. The code is currently operational on the Sandia CDC6600/7600 system, the CRAY and VAX11/780 computers.

Comparison of the code results with the SMRI solution mining code SALT77, show good agreement for small caverns in which the injection point is near the top of the cavern and the brine production is at the bottom or vice versa. The simulation of the development of large SPR caverns has been fairly successful. Almost all of the volume comparisons are within 5% despite raw water temperature fluctuations, cavern asymmetries, and uncertainties in the flow measurements and' insolubles distribution. Local deviations in radius of up to 20% have been seen in several caverns, however. It appears that improvements in the flow and dissolution models as well as tighter control of the input variables will be necessary to improve the predictive accuracy of the code.

SANSMIC users are CAUTIONED that the models employed in this code are steady-state or quasi-steady models and that the code has only been verified with experimental data from SPR caverns which have large length-to-diameter ratios. These caverns were leached with flow rates in the 10^5 barrel per day range. Operation in a different flow rate or geometry range may not give similar accuracy. In particular, laboratory and field experience indicates that water injected in short bursts, after which the enclosure is allowed to stabilize, rises to the top of the enclosure with little mixing and tends to etch out a narrow disk just below the blanket or pad. SANSMIC will not model this behavior properly.

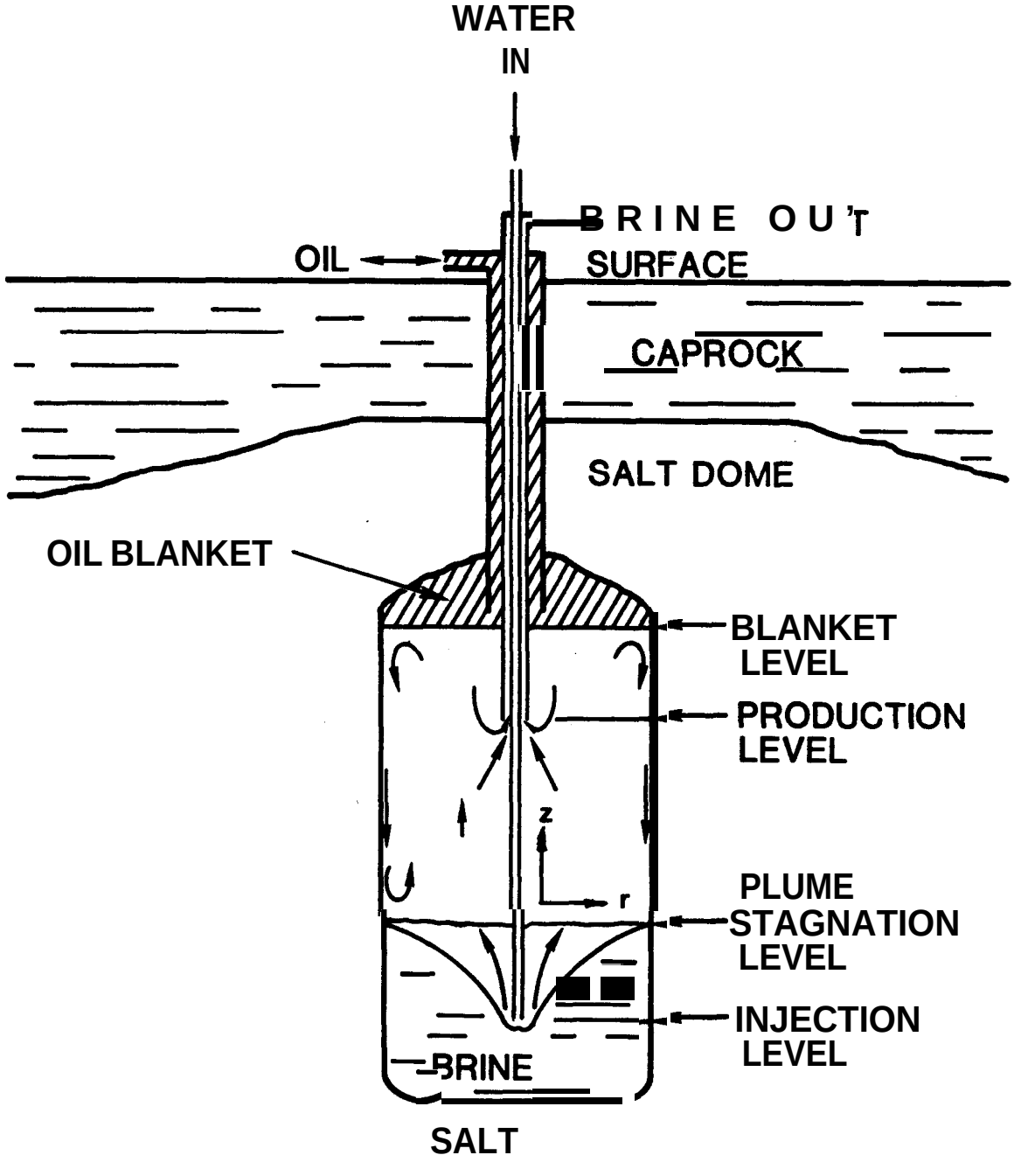

Figure 1. Cavern Geometry and Flow Regions for Direct Leaching

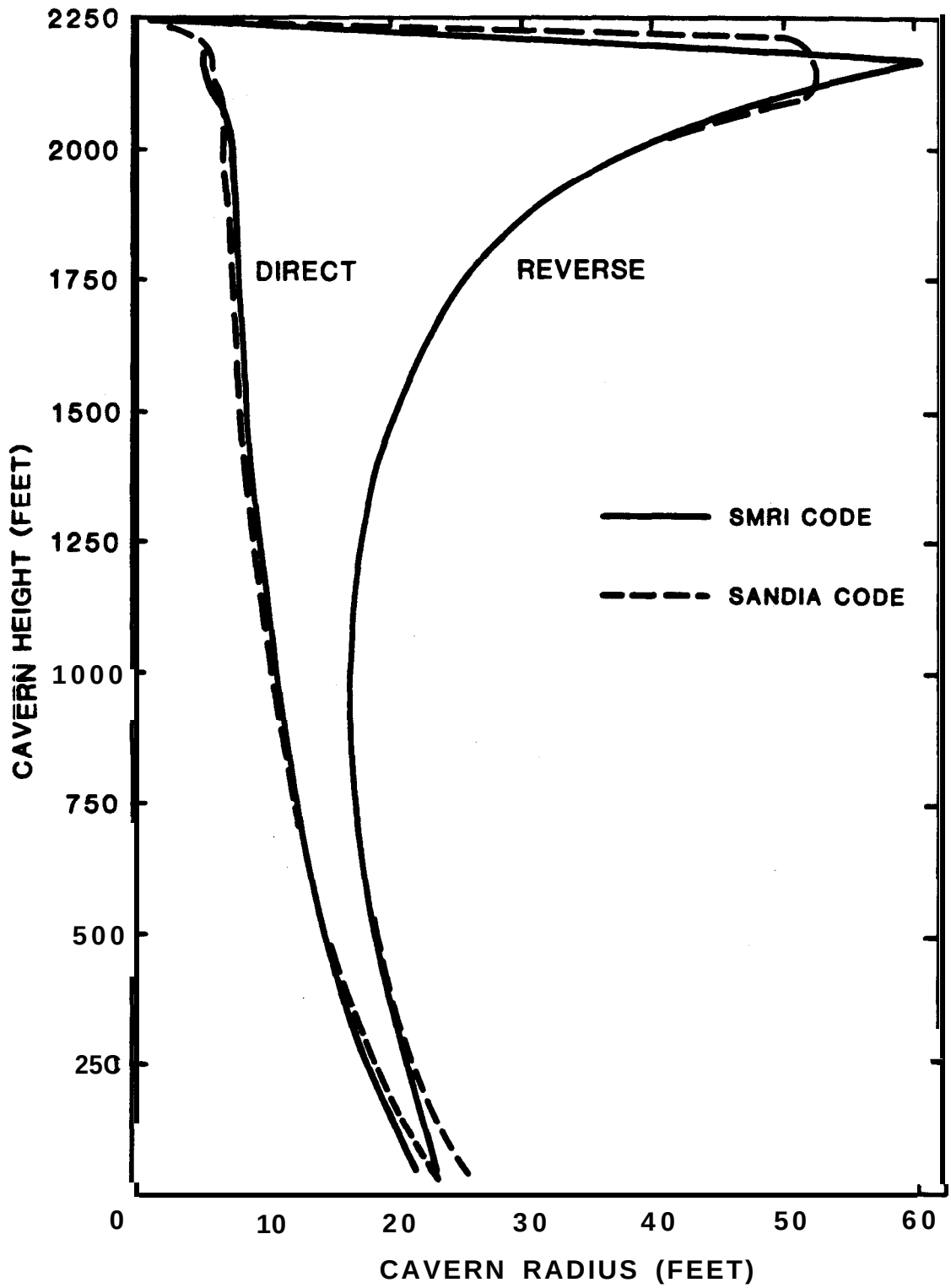

Figure 2. A Comparison of Calculated Cavern Shapes

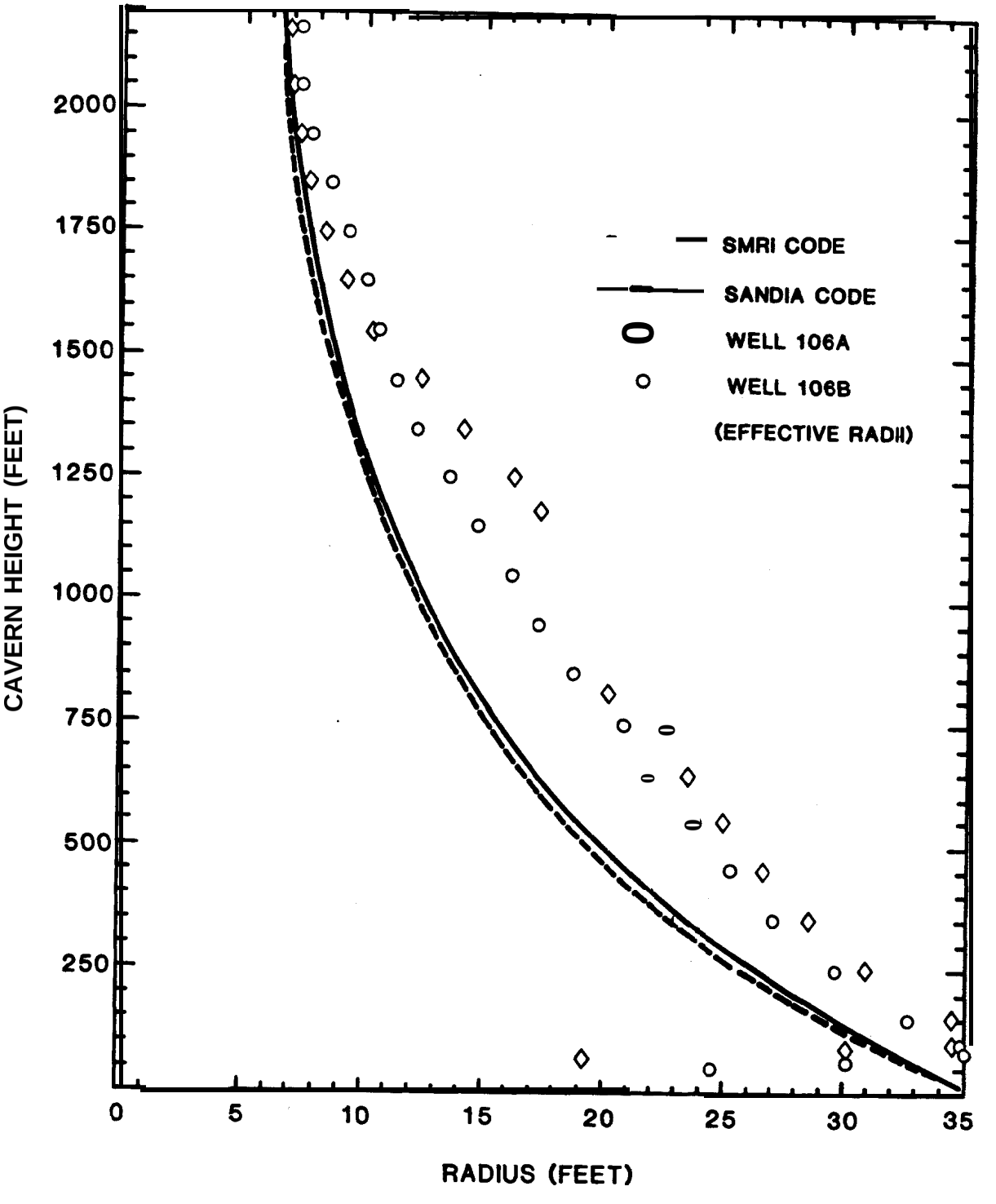

Figure 3. A Comparison of Calculated and Measured Cavern Shapes for Bryan Mound Cavern 106

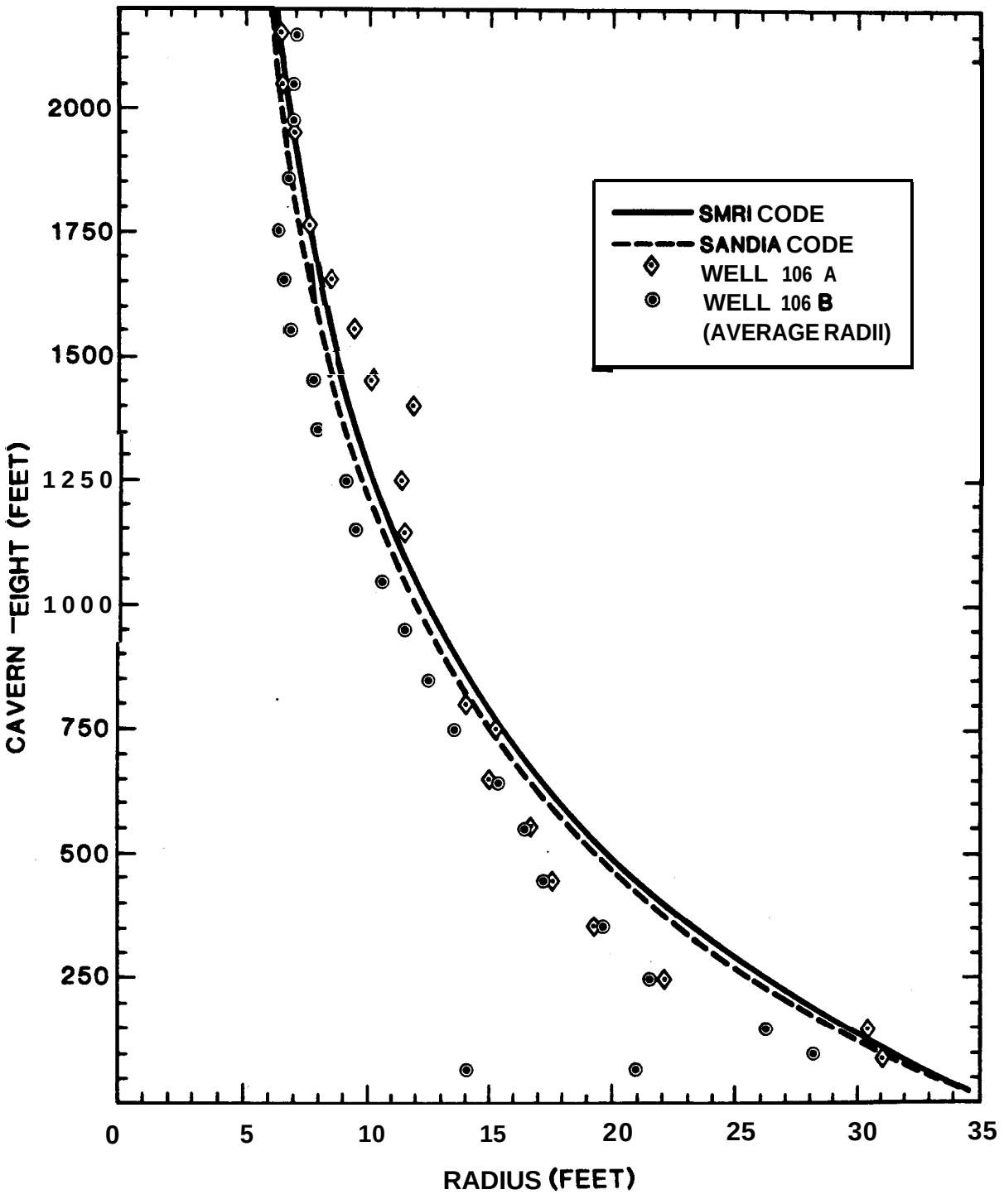

Figure 4. A Comparison of Calculated and Measured Shapes for Bryan Mound Cavern 106

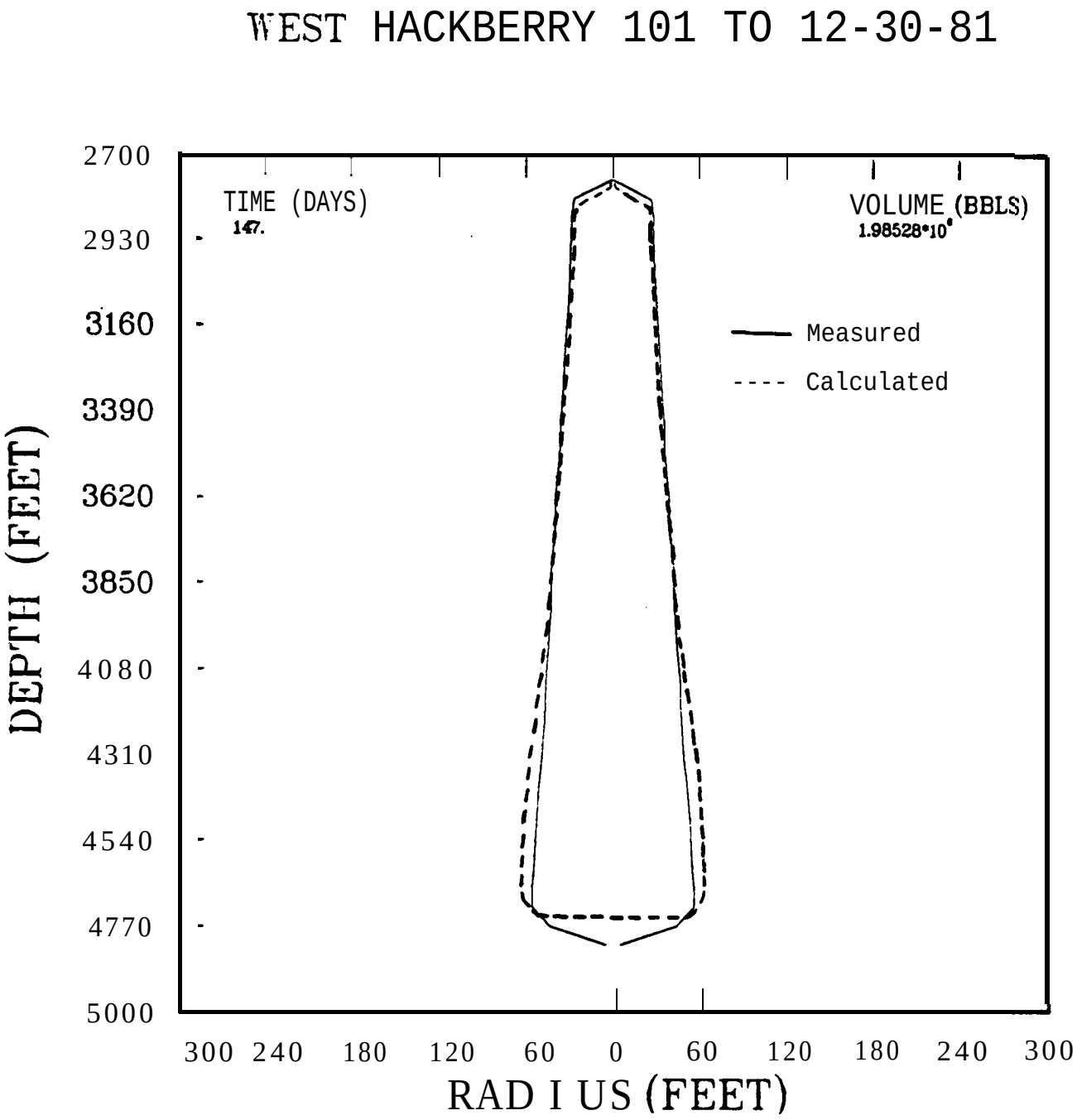

Figure 5. **A Comparison of Calculated and Measured Cavern Shapes after Direct Leaching of WH101**

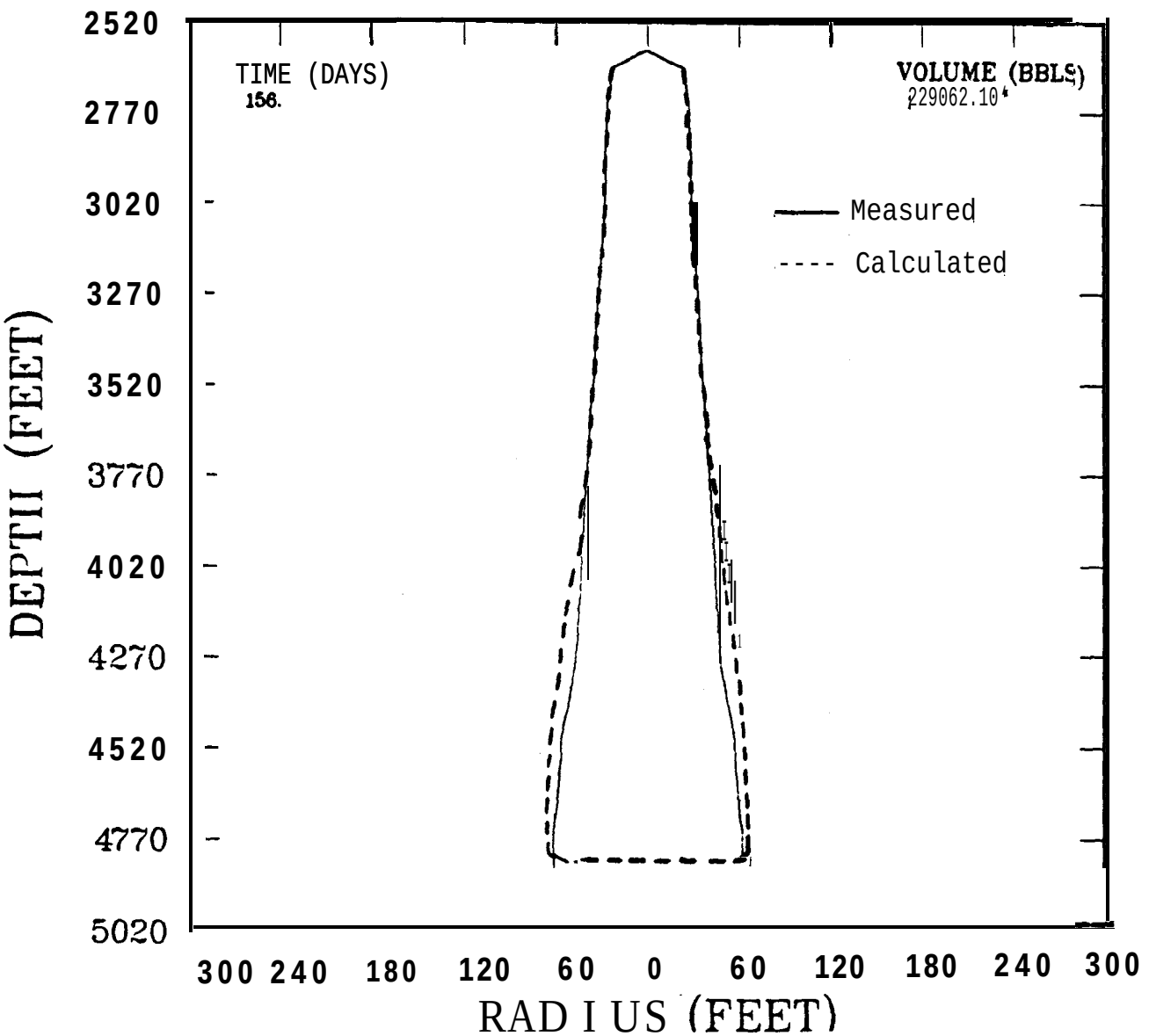

Figure 6. A Comparison of Measured and Calculated Cavern Shapes after Direct Leaching of WH104

WEST HACKBERRY 101 FROM 12/81 TO 7/82

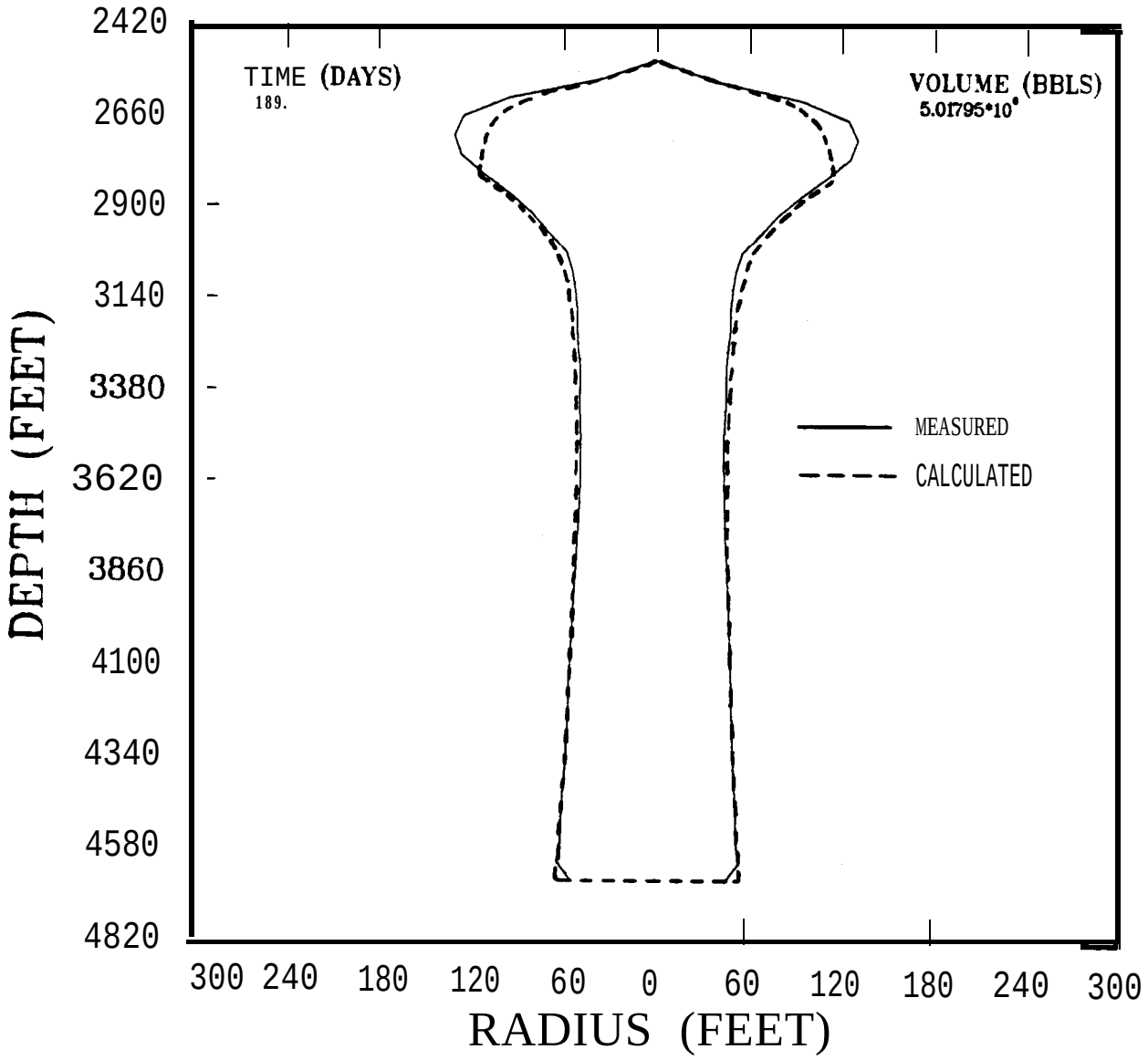

Figure 7. A Comparison of Calculated and Measured Cavern Shapes after Reverse Leaching of WH101

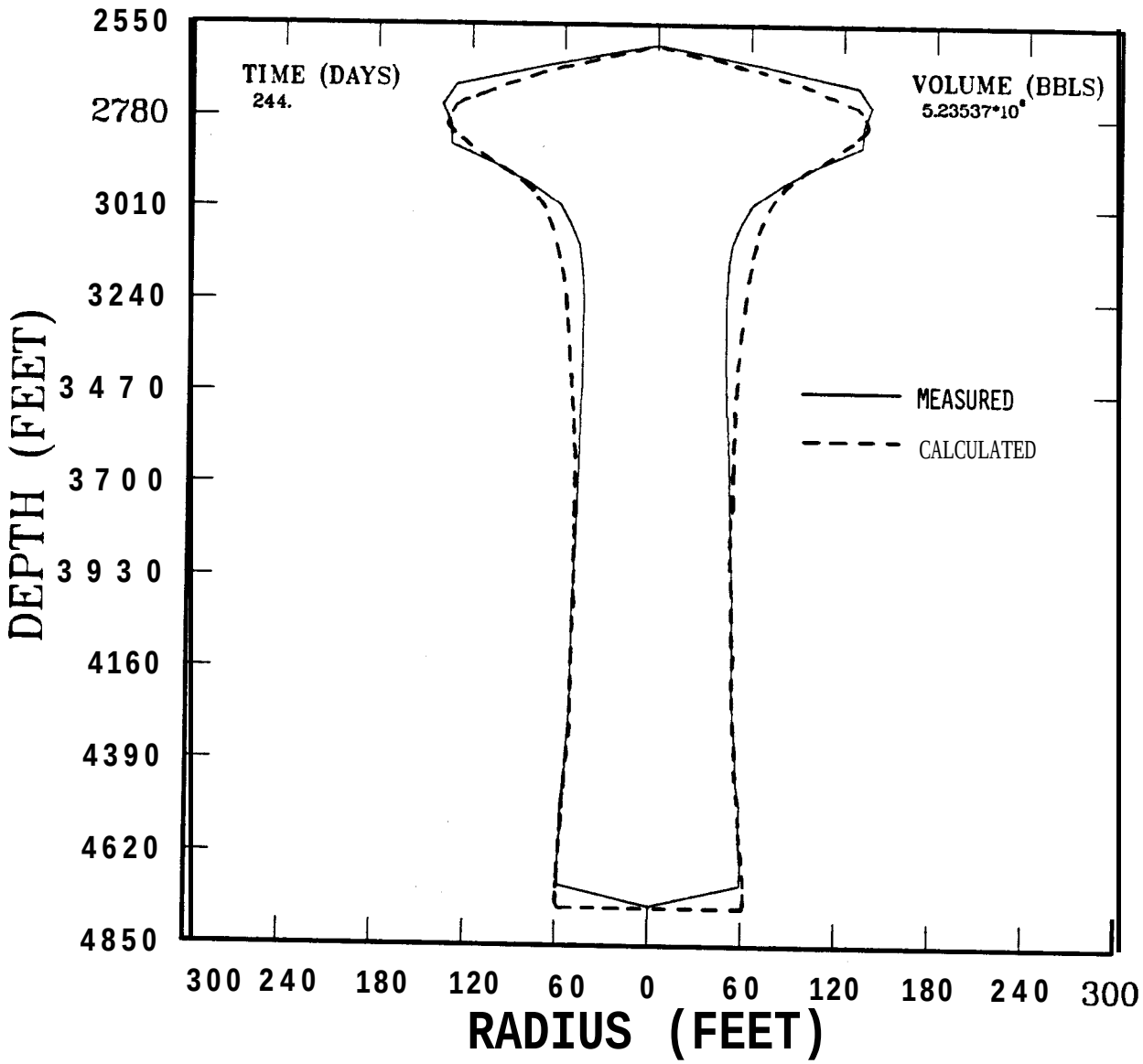

Figure 8. A Comparison of Calculated and Measured Cavern Shapes after Reverse Leaching of **WH104**

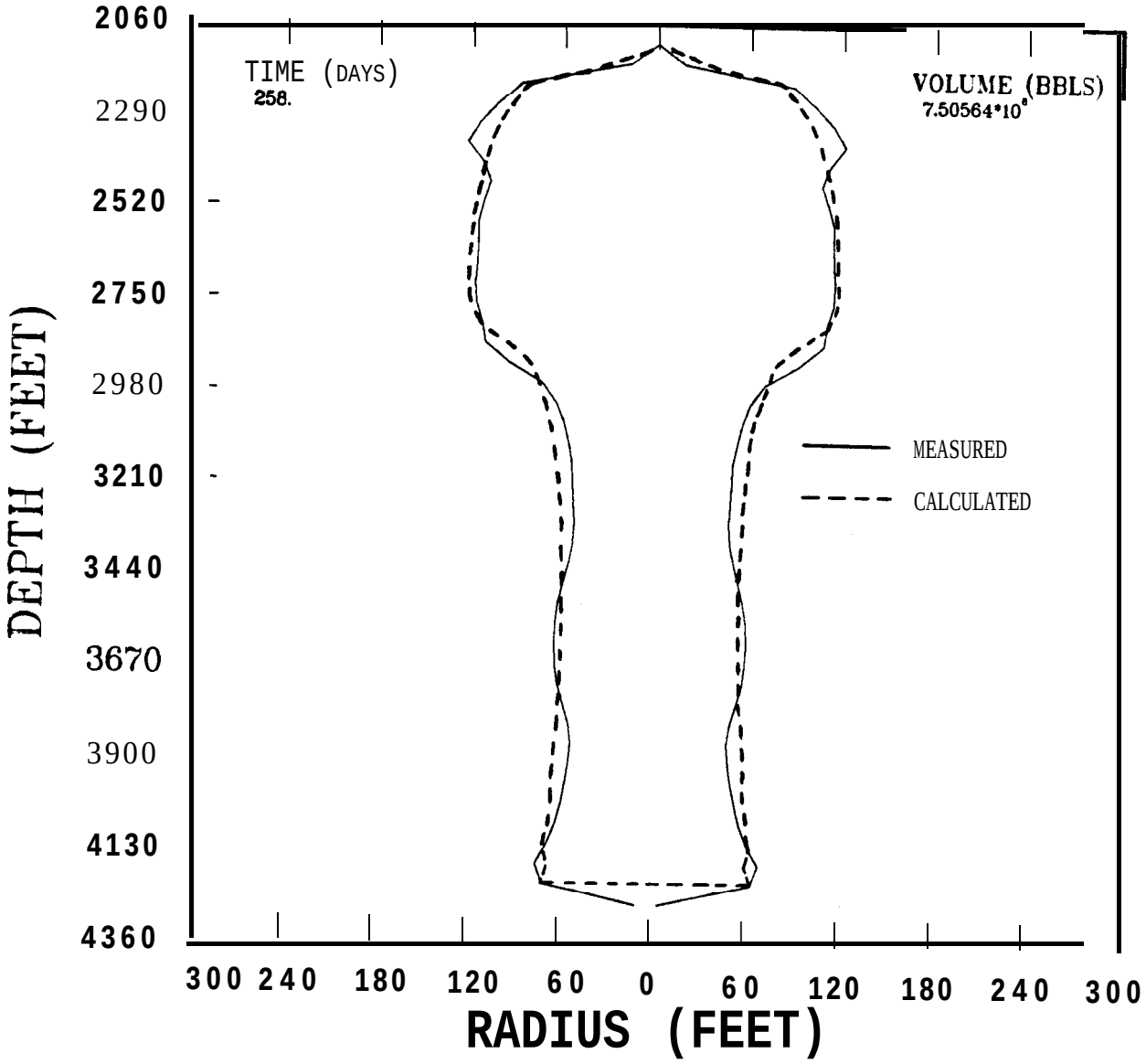

Figure 9. A Comparison of Calculated and Measured Cavern Shapes after Reverse Leaching of BM106

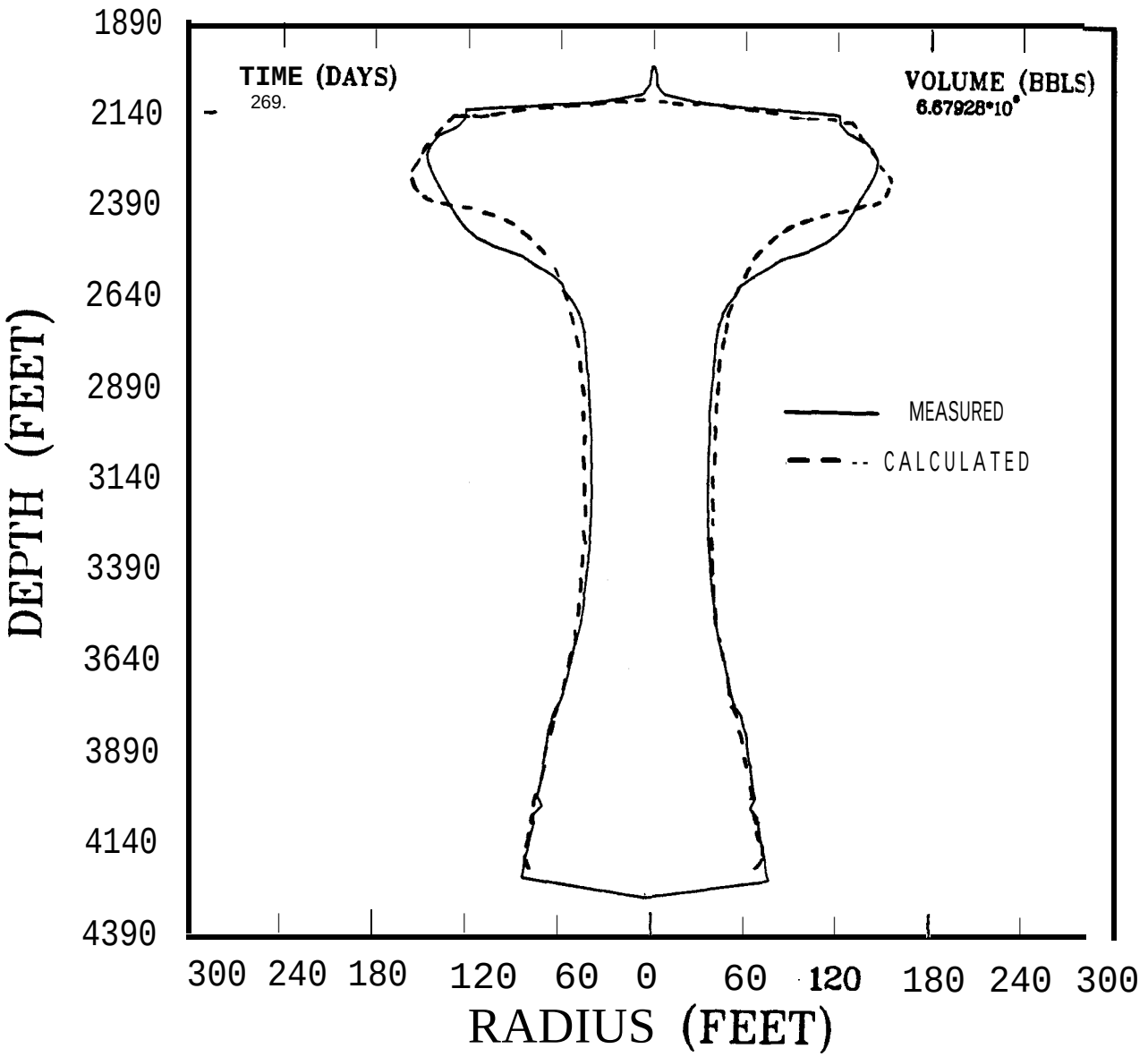

Figure 10. A Comparison of Measured and Calculated Cavern Shapes after Reverse Leaching of BM106

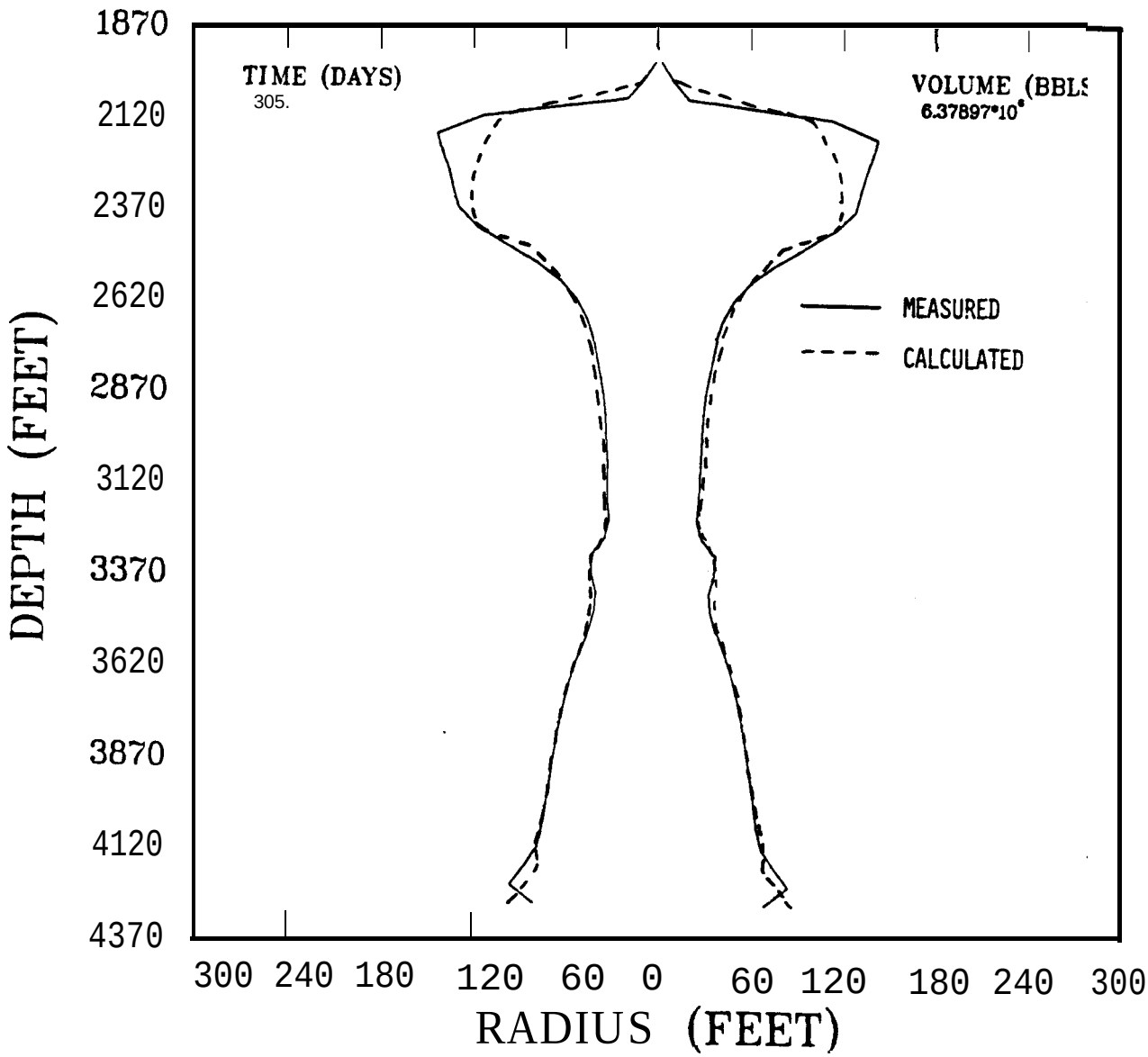

Figure 11. A Comparison of Measured and Calculated Cavern Shapes after Reverse Leaching of **BM105**

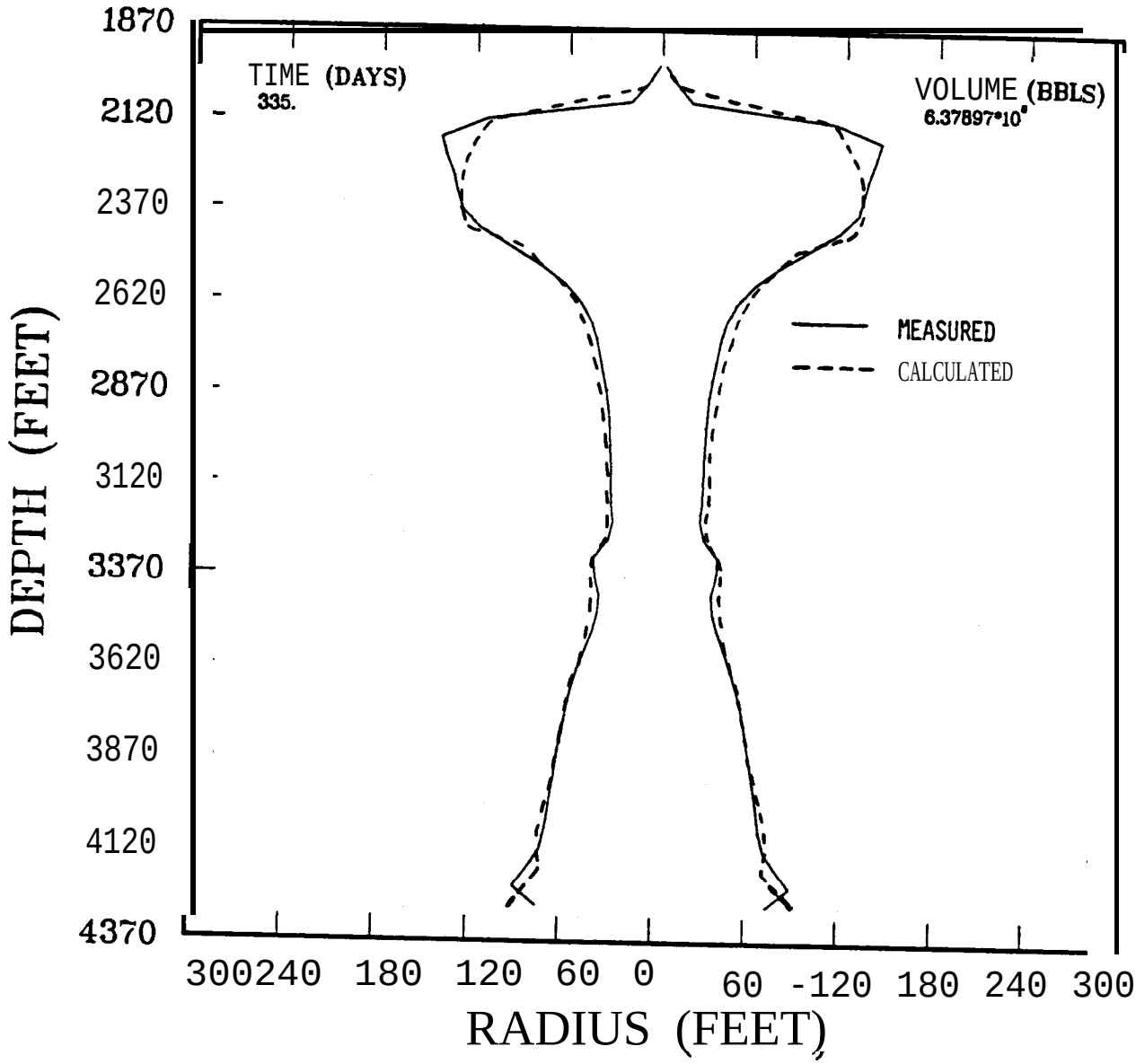

Figure 12. **A Comparison of Measured and Calculated Cavern Shapes (with Corrected Flow Rates) after Reverse Leaching of BM105**

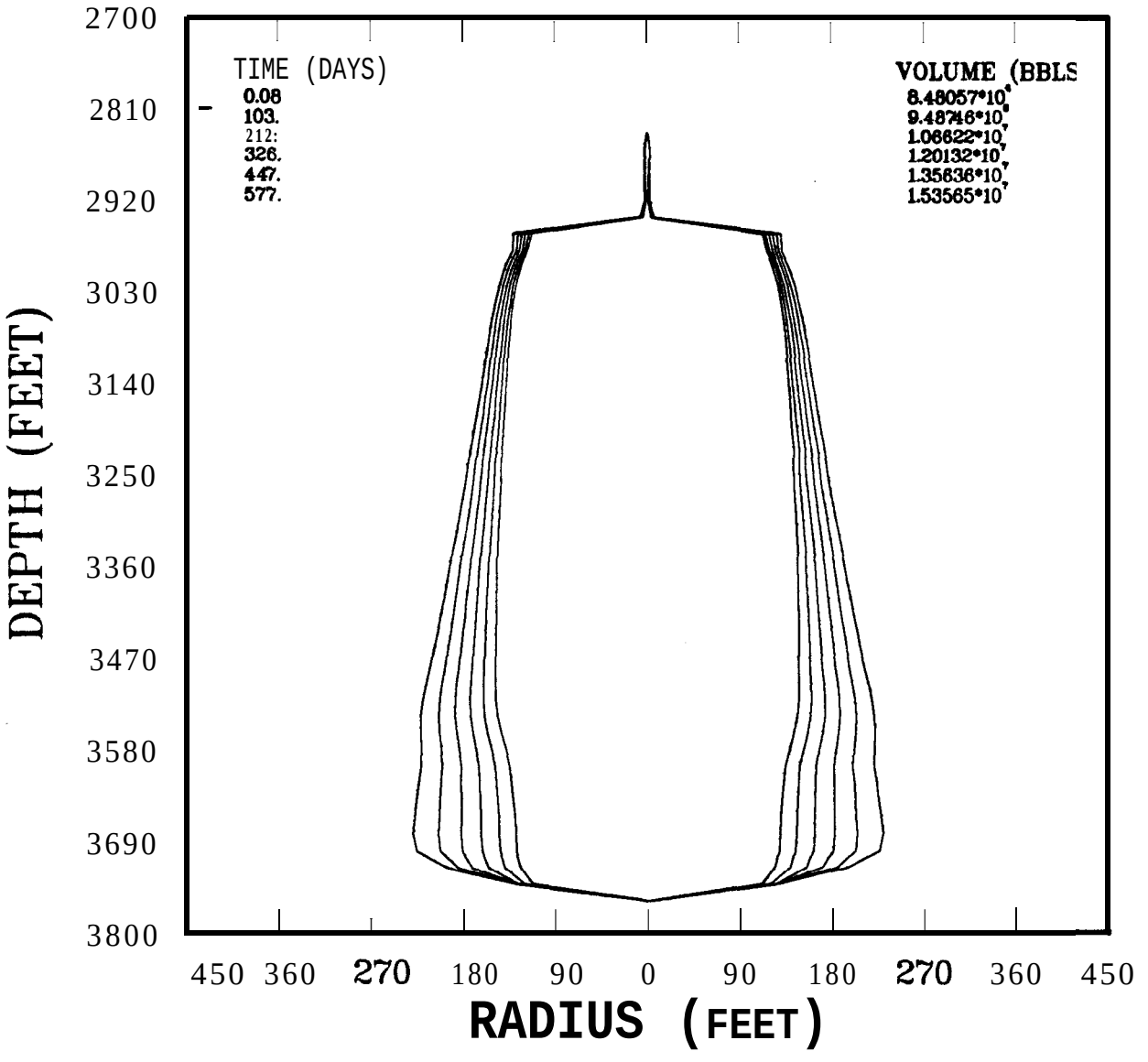

Figure 13. An Example of Calculated Cavern Enlargement for Five Oil Withdrawal Cycles

```
WEST HACKBERRY 101 FROM 12/81 TO 7/82 $
  46    0   50    0    0    0    0    0    0
2300.0    2020.0     120.0    2300.0    153000.0  3.75      4.25      6.18
6.68      1.0025     1.2      3.0       936.0     0.0       0.0       0.0
    5.00      43.72     55.99     56.17     54.85     54.14     53.51     52.68
   51.82      50.53     49.14     48.13     47.21     46.76     46.43     45.41
   44.24      43.46     42.56     42.43     42.47     41.30     39.86     39.40
   39.19      38.07     36.72     36.24     35.97     34.81     34.02     33.33
   32.65      31.80     30.88     30.04     29.55     an.11     28.73     28.54
   26.98       0.63      0.63      0.63      0.63      9.63      0.63      0.63
1.0       0.05      4826.8    4826.8
 FIRST REVERSE $
  46    0   42    1  128%    0    0    0    0
2300.0    2020.0               2300.0    78000.0   3.75      4.25      6.18
6.68      1.0025     1.2       3.0       168.0     0.0       0.0       0.0
 FIRST REVERSE $
  46    0   25    1    0    0    0    0    0
2300.0    2020.0     120.0     2300.0    135000.0  3.75      4.25      6.18
6.68      1.0025     1.2       6.0       336.0     0.0       0.0       0.0
 FIRST REVERSE $
  46    0   21    1    0    0    0    0    0
2300.0    2020.0     120.0     2300.0    122000.0  3.75      4.25      6.18
6.68      1.0025     1.2       6.0       216.0     0.0       0.0       0.0
 FIRST REVERSE $
  46    0   50    1    0  288    0    0    0
2300.0    2020.0     120.0     2250.0    142625.0  3.75      4.25      6.18
6.68      1.0025     1.2       6.0       768.0     0.0       0.0       0.0
 FIRST REVERSE $
 -46    0   40                   0    0    0
2366.6    2020.0     1  128%    02250.0   141792.0  3.75      4.25      6.18
6.68      1.0025     1.2       6.6       240.0     0.0       0.0       0.0
 FIRST REVERSE $
  46    0   50    1    0    0    0    0    0
2300.0    2020.0     120.0     2200.0    125000.0  3.75      4.25      6.18
6.68      1.0025     1.2       6.6       552.0     0.0       0.0       0.0
 FIRST REVERSE $
  46    0   50    1    0  648    0    0    0
2300.0    2020.0     126.6     2200.0    72335.0   3.75      4.25      6.18
6.68      1.0025     1.2       6.0       384.0     0.0       0.0       0.0
$
```

Figure 14. Sample Input Data for SANSMIC

TIME• 25.13 DAYS DT• 3.00 HOURS START TIRE= 0.00 DAYS

HEIGHT	RADIUS	BRINE S.G.	UALL ANGLE	FLOU RATE	VOLUME
2300.0	0.63	1.1088	180 00	0.00	11.10
2250.0	27.69	1.1088	105.82	0.00	21466.36
2200.0	29.10	1.1069	92.42	-153000.02	45164.97
2150.0	31.92	1.1069	92.95	-153000.02	73665.86
2100.0	34.25	1.1069	92.05	-153000.02	106483.93
2050.0	35.42	1.1069	97.24	-153000.02	141709.52
2000.0	46.89	1.1069	96.53	-153000.02	203211.91
1950.0	46.88	1.1169	88.63	-153000.02	264686.75
1900.0	44.49	1.1248	86.94	-153000.02	320053.00
.--1850	41.51	1.1303	87.32	-153000.02	368267.75
1751800	39.78	1.1346	88.44	-153000.02	412537.81
	38.78	1.1382	89.29	-153000.02	454606.38
17ee.o	38.53	1.1414	89.92	-153000.02	496156.22
1660.9	38.62	1.1442	96.16	-153000.02	S3788S.66
1600.0	38.81	1.1468	90.09	-153000.02	580015.50
1550.0	38.77	1.1490	90.15	-153000.02	628e77.88
1500.0	39.07	1.1512	98.41	-153000.02	664779.66
1450.0	39.49	1.1532	96.71	-153000.02	708410.63
1400.0	40.30	1.1552	96.44	-153000.02	753857.SC
1350.0	40.26	1.1570	99.68	-153000.02	799197 .50
1300.0	49: 4s	1.1587	90.73	-153000.02	844975.63
1250.0	41.53	1.1604	91.11	-153000.02	89323.. 50
1200.0	42.39	1.1619	90.48	-153000.02	943Se7.63
1150.0.	42.37	1.1634	90.13	-153000.02	993730. 00
1100.0	48.61	1.1648	90.89	-153000.02	1044537.66
1050.0	43.85	1.1662	91.27	-153666.62	1098344.25
1000.0	44.83	1.1679	90.44	-153000.02	1154577.88
966.e	44.62	1.1688	89.86	-153000.02	1210277.38
9ee.e	44.59	1.1699	90.42	-153000.02	1265910.13
850.0	45.35	1.1711	90.80	-153000.02	1323443.7s
800.0	45.99	1.1722	96.97	-153000.02	1362621.63
750.0	47.03	1.1732	91.11	-153000.02	1444510.13
700.0	47.93	1.1743	90.64	-153000.02	1508787.25
650.0	48.15	1.1752	96.33	-153000.02	lS736S2.38
600.0	48.50	1.1762	9e.67	-153000.02	1639466.38
550.0	49: 33	1.1771	91.00	-153000.02	1707529.50
500.0	50.25	1.1779	91.28	-1S3OeO.62	1778164.13
450.0	51.55	1.1788	91.44	-153000.02	1852519.75
400.0	52.76	1.1796	91.14	-153000.02	1930406.13
350.0	s3: ss	1 1804	98.89	-153000.02	2010625.63
300.0	54.31	1.1811	90.76	-153000.02	2093143.00
250.0	S4.87	1.1818	90.70	-153000.02	2177387.25
200.0	55.53	I.1825	91.10	-153000.02	2263644.66
150.0	56.79	1.1832	90.59	-153000.02	2353871.06
100.0	56.56	1.1839	82.58	-153000.02	2443360.75
50.0	43.76	1.2018	62.73	0.00	2496926.25
0.0	5.00	1.2019	52.23	0.00	2497626.25

TOTAL VOLUME• 2473249.5 BBLS BRINE OUT= 147504.58 BBLS/DAY
OUTLET SPECIFIC GRAVITY• 1.1839

VOLUME O F INSOLUBLES• 24398.6. BBLS INSOL LEVEL• 72.12 FT
BLANKET LEVEL• 2300.00 CT UOL OF INS VENTED• 0.00 BBLS

BRINE VOLUME• 2473249.50 BBLS CFAC• 0.9990140

Figure 15. A Sample SANSMIC Output Page

REFERENCES

1. Saberian A. and Podio A. L., "A Computer Model for Describing the Development of Solution-Mined Cavities, IN SITU, l(l), p. l-36 (1977).
2. Russo, A. J., "A Solution Mining Code For Studying Axisymmetric Salt Cavern Formation", Sandia Report SAND81-1231, September, 1981
3. Durie R. N. and Jessen F. W., "Mechanism of the Dissolution of Salt in the Formation of Underground Salt Cavities," SPE Journal, p. 183, (June, 1964).
4. Durie R. N. and Jessen F. W., "The Influence of Surface Features in the Salt Dissolution Process", SPE Journal, p. 275 (September, 1964).
5. Kreith F., Principles of Heat Transfer, International Textbook Co. Scranton, p. 310, (1958).
6. Rahm L. and Walin G., "On Thermal Convection in Stratified Fluids", Geophys. Astrophys. Fluid Dynamics, V 13, p. 51, (1979).
7. Rahm L. and Walin G., "Theory and Experiment on the Control of the Stratification in Almost Enclosed Containers", J. Fluid Mech. 90, p. 315 (1979).
8. Walin G., "Contained Non-Homogeneous Flow Under Gravity or How to Stratify a Fluid in the Laboratory", J. Fluid Mech. 48, p. 647, (1971).
9. Morton B.R. et al.; "Turbulent Gravitational Convection from Maintained and Instantaneous Sources", Proc. of the Royal Society, Series A, Vol. 234, No. 1196, Jan 24, p. 1, (1956).
10. Knapp R.M. and Podio A.L., "Investigation of Salt Transport in Vertical Borholes and Brine Invasion into Fresh Water Aquifers", ONWI-77 (May, 1979).

Distribution:

E. E. Chapple, PMO-681 (6)
U. S. DOE SPRPMO
900 Commerce Road East
New Orleans, LA 70123

L. Rousseau
U. S. DOE SPRPMO
900 Commerce Road East
New Orleans, LA 70123

V. Kilroy
U. S. DOE SPRPMO
900 Commerce Road East
New Orleans, LA 70123

Larry Pettis
U. S. Department of Energy
Strategic Petroleum Reserve
1000 Independence Avenue, SW
Washington, DC 20585

Bill Wilson
U. S. Department of Energy
Strategic Petroleum Reserve
1000 Independence Avenue, SW
Washington, DC 20585

Aerospace Corporation (2)
800 Commerce Road East, Suite 300
New Orleans, LA 70123
Attn: E. Katz
R. Merkle

Jacobs/D'Appolonia Engineers (2)
P. 0. Box 23308
Harahan, LA 70183
Attn: P. Campbell
H. Kubicek

POSSI (2)
850 S. Clearview Pkwy.
New Orleans, LA 70123
Attn: Dub Butler

W. Marquardt
Parsons-Gilbane
800 Commerce Road West
New Orleans, LA 70123

Alfred H. Medley
Fenix & Scisson, Inc
1401 South Boulder
Tulsa, OK 74119

Dr. Alfred Finkenwirth
LANZSTR.25
6200 Wiesbaden
West Germany

Gayle D. Petrick, P.E.
Diamond Crystal Salt Company
St. Clair, MI 48079

Eng. Diamantino Mendonca
Socio-Gerente
Sondagens E Fundacoes A. Cavaco, LDA.
Av. Eng. Durate Pacheco, 21-2.°
1000 Lisboa
Portugal

Ir. Th. H. Wassmann
Manager, Minerals Department
Akzo Zout Chemie Nederland bv
Boortorenweg 20
7554 RS Hengelo (0)
The Netherlands

Jerome S. Blank
Kalium Chemicals
Suite 1120
600 South Cherry Street
Denver, CO 80222

Joseph Didier Martinez, CPGS, PE
P. 0. Drawer J.D.
University Station
Baton Rouge, LA 70893

Elmar L. Goldsmith
Kalium Chemicals
400 Bank of Canada Building
Regina, Saskatchewan S4P 0M9
Canada

Distribution:

Hans Y. Tammemagi, PhD
RE/SPEC Ltd.
Suite 201
4616 Valiant Drive, NW
Calgary, Alberta T3A OX9
Canada

Hans-J. Doering
Ruhrgas Aktiengesellschaft
Referent Technische Planung - Lagerstatten
Huttropstrasse 60
D-4300 Essen 1
West Germany

Dr. Adrian J. Van Der Iioeven
lord-west Xavernengesellschaft
MIT Beschrankter Haftung
2940 Wilhelmshaven 31
Xavernenfeld X-6
West Germany

James Ii. Huizingh
Texasgulf Chemicals Co.
P. 0. Box 1208
Moab, UT 84532

E. Leon Cook
PPG Industries, Inc.
P. 0. Box 1000
Lake Charles, LA 70602

A. Saberian and Associates
3305 Northland Drive #407
Austin, TX 78731

1510 D. B. Hayes
1512 J. C. Cummings
1512 A. J. Russo (10)
1513 M. R. Baer
1513 R. J. Gross
1520 W. Herrmann (Acting)
1530 L. W. Davison
1540 W. C. Luth
6257 J. K. Linn (6)
8214 M. A. Pound
3141 L. J. Erickson (5)
3151 W. L. Garner (3)
For DDE/TIC (Unlimited Release)
3154-3 C. H. Dalin (25)
DDE/TIC